JAAS

PAPER

View Article Online
View Journal | View Issue

Cite this: J. Anal. At. Spectrom., 2015, 30, 627

The mapping and differentiation of biological and environmental elemental signatures in the fossil remains of a 50 million year old bird

Victoria M. Egerton,*[a] Roy A. Wogelius,[a] Mark A. Norell,[b] Nicholas P. Edwards,[a] William I. Sellers,[c] Uwe Bergmann,[d] Dimosthenis Sokaras,[e] Roberto Alonso-Mori,[d] Konstantin Ignatyev,[f] Arjen van Veelen,[a] Jennifer Anné,[a] Bart van Dongen,[a] Fabien Knoll[a] and Phillip L. Manning[ab]

The preservation of fossils reflects the interplay of inorganic and organic chemical processes, which should be clearly differentiated to make interpretations about the biology of extinct organisms. A new coliiformes bird (mouse bird) from the ~50 million year old Green River Formation (Wyoming, USA) has here been analysed using synchrotron X-ray fluorescence and environmental scanning electron microscopy with an attached X-ray energy dispersive system (ESEM-EDS). The concentration and distribution of 16 elements (Si, P, S, Cl, K, Ca, Ti, Mg, Fe, Ni, Cu, Zn, As, Br, Ba, Hg) has been mapped for individual points on the sample. S, Cu and Zn map distinctly within visibly preserved feathers and X-ray Absorption Spectroscopy (XAS) shows that S and Cu within the feathers are organically bound in a similar manner to modern feathers. The morphological preservation of the feathers, on both macro- and microscopic scales, is variable throughout the fossil and the differences in the lateral microfacies have resulted in a morphological preservation gradient. This study clearly differentiates endogenous organic remains from those representing exogenous overprinted geochemical precipitates and illustrates the chemical complexity of the overall taphonomic process.

Received 31st October 2014
Accepted 16th January 2015

DOI: 10.1039/c4ja00395k

www.rsc.org/jaas

1. Introduction

Fossils are formed through a complex system of physical and chemical changes that begin at the moment of an organism's death. Taphonomy (literally 'burial-laws') is the study of such changes and interactions on the buried remains of an organism. The taphonomic changes are controlled by the environment in which the organism is buried and by the biological tissues constructing the organism. Mineralized or 'hard' tissue, like bone, shell, and teeth, are more easily preserved due a combination of their crystalline structure and chemistry.[1] However, soft tissue preservation is rare and restricted to a narrow selection of environmental regimes. In terrestrial environments, exceptional preservation can occur in lacustrine (lake) environments due to the low energy and reduced-oxygen conditions in such depositional systems.[1,2] Reduced oxygen helps to inhibit bacterial activity and tissue decay while favouring mineral precipitation around the tissues of the organism.[1,3]

The Green River Formation consists of limestone deposits extending over 65 000 square kilometers across Utah, Colorado, Wyoming and Idaho.[4] The Formation consists of a series of three Eocene lakes: Uinta, Gosiute and Fossil Lakes. Supersaturation of calcium carbonate within the lakes from rivers flowing from the proto-Rocky Mountains caused the deposition of this carbonate succession. A diverse community of mammals, birds, reptiles, amphibians and fishes that lived in and around the have been preserved in this carbonate succession. Local reduced oxygen conditions within the lakes facilitated the preservation of these organisms.[4] Here we discuss the excellent preservation of an Eocene Coliiformes bird and examine the complexity of its preservation from a standpoint of both the endogenous biochemistry and exogenous geochemistry.

2. Methods

2.1. Sample

The fossilized remains of a mousebird (Coliiformes) (Fig. 1) were examined from the collections of the American Museum of Natural History, New York, USA (AMNH FARB 30806). This

[a]University of Manchester, School of Earth, Atmospheric and Environmental Sciences, Williamson Research Centre for Molecular Environmental Science, Manchester M13 9PL, UK. E-mail: victoria.egerton@manchester.ac.uk
[b]American Museum of Natural History, Division of Paleontology, New York 10024-5192, USA
[c]University of Manchester, Faculty of Life Sciences, Manchester M13 9PL, UK
[d]SLAC National Accelerator Laboratory, Linac Coherent Light Source, Menlo Park, CA, 94025, USA
[e]SLAC National Accelerator Laboratory, Stanford Synchrotron Radiation Lightsource, Menlo Park, CA 94025, USA
[f]Diamond Light Source, Didcot, OX11 0DE, UK

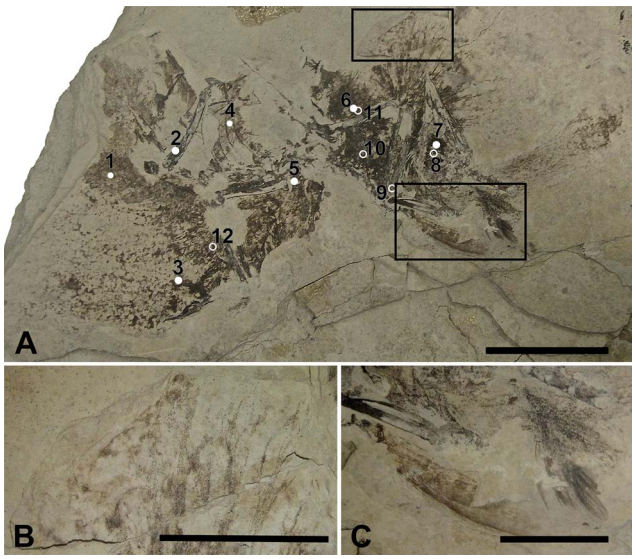

Fig. 1 AMNH FARB 30806. (A) Coliiformes bird (AMNH FARB 30806) from the Green River Formation, Fossil Butte Member. The numbers correspond to where point data was taken for high *Z* (1–7) and low *Z* (8–12) elements. Scale bar = 5 cm. (B) Magnified view of the upper box containing the feather sample obtained for SEM. (C) Magnified view of well preserved feathers. (B and C) Scale bar = 2 cm.

specimen was collected from the ~50 million year old Fossil Butte Member (Fossil Lake) of the Green River Formation, on the Lewis Ranch, Lincoln County, Wyoming AMNH FARB 30806 was not subjected to any chemical preparation procedures (including glues and consolidants) post collection to prevent chemical contamination. A small piece of the distal tip of a left primary wing feather was removed for scanning electron microscopy (Fig. 1b). To minimise damage to the fossil, this area was chosen because of a natural break in the slab. The sample was not destroyed and remains with the main slab.

2.2. Synchrotron X-ray fluorescence and X-ray absorption spectroscopy

Synchrotron analyses were undertaken at Stanford Synchrotron Radiation Lightsource (SSRL) beam line 6-2 and at Diamond Light Source (DLS) beam line I18. Our experimental setup and methods for the analysis of samples at these two facilities has been discussed extensively in previous studies.[5–12] Additionally, Bergmann *et al.*[12] provides a comprehensive review of the techniques applied in this study. Analysis of AMNH FARB 30806 replicated the methods in these studies; a summary of those methods is discussed below.

Synchrotron Rapid Scanning X-ray Fluorescence (SRS-XRF) at SSRL wiggler beam line 6-2 has been optimized to perform 2D elemental imaging on the scale of decimeters at a resolution of 100 microns or less with an acquisition rate of about 30 s cm^{-2}. This allows entire surfaces of specimens (fossil or otherwise up to 60 × 60 cm) to be elementally mapped. SRS-XRF is particularly useful for fossils as they can be analysed *in situ* with their embedding geological matrix without necessitating destructive sampling. This technique allows for elemental distributions affiliated with biological or geological processes to be visualized. A single element Vortex silicon drift detector was employed, which can detect the X-ray emissions of up to 16 elements simultaneously allowing those elements to be spatially mapped. For this experiment the elements that were mapped across the fossil and matrix included: silicon, phosphorus, sulfur, chlorine, potassium, calcium, titanium, manganese, iron, nickel, copper, zinc, arsenic, bromine, barium and mercury. The incident beam energy for the XRF imaging experiments was 13.5 keV optimized for detecting the K-edge emission of elements of atomic number 20 (Ca) to 80 (Hg) and performed under ambient conditions (high *Z*). Lower atomic number elements (low *Z*) from 14 (Si) to 17 (Cl) were scanned at a beam energy of 3.15 keV with specimens enclosed within a helium atmosphere to reduce attenuation of the incident beam and fluoresced signal. A beam diameter of 100 μm was achieved using a tantalum pinhole. Spatial correlations from the elemental maps were processed using ImageJ[13] utilizing the Image CorrelationJ[14] plugin.

Quantification and X-ray Absorption Near Edge Structure (XANES)[15] spectroscopy of S and Cu were also conducted at SSRL. Quantification was conducted under the same experimental conditions as the elemental maps with a full Energy Dispersive Spectrometry (EDS) spectrum collected for 100 live seconds for each location. Points were taken in both high *Z* and low *Z* geometries on a number of matrix and fossil tissue types for quantitative analysis of AMNH FARB 30806 (Fig. 1a). The point analyses were fitted using PyMCA freeware[16] and calibrated against a mineral (Durango apatite) reference standard.

XANES spectroscopy at the S Kα edge and the Cu Kα edge were conducted to determine oxidation states. Sulfur (K_2SO_4) and copper (Cu foil) standards were used to calibrate the energy of the monochromator position. The sulfate peak position (2481.75 eV) was based on the K_2SO_4 standard. Organic sulfonate (2480.25 eV), sulfoxide (2474.35 eV) and thiol (2473.25 eV) were calibrated on the K_2SO_4 standard and from published data.[5,8,17,18]

Extended X-ray Absorption Fine Structure (EXAFS)[15] spectroscopy at the Mn Kα edge was conducted at the Diamond Light Source (DLS) beamline I-18 using Kirkpatrick-Baez mirrors to produce a beam spot size of 5 microns. EXAFS spectroscopy was conducted in order to ascertain the coordination chemistry of Mn.

2.3. Environmental Scanning Electron Microscopy (ESEM) with Energy Dispersive Spectroscopy (ESEM-EDS)

ESEM images and EDS quantification were acquired using a JEOL JSM-6400 with energy dispersive X-ray (EDX) spectroscopy (Princeton Gamma Tech system). The sample was uncoated and imaged in partial vacuum using backscatter or secondary electron detectors at an accelerating voltage of either 12 or 15 keV. Semi-quantitative standard-less EDS analyses was completed using an accelerating voltage of 15 keV for 100 live seconds.

3. Results

Feather preservation in AMNH FARB 30806 is variable, with some feathers well preserved (Fig. 1c), while others have clearly

decomposed (Fig. 1a). Fig. 1c shows one of the well-preserved feathers with gradational preservation from well preserved with clear barbs to more patchy organic areas in the general form of feathers. The fossil appears to exhibit differences in lateral microfacies that resulted in a morphological preservation gradient or 'morpho-gradient'.

3.1. Synchrotron X-ray Fluorescence and X-ray Absorption Spectroscopy

SRS-XRF maps of AMNH FARB 30806 reveal that particular elements are constrained within discrete biological structures while others follow a distribution consistent with geological processes. Elements such as P, S, Ca, Cu and Zn occur within bones, feathers and the orbit (eye socket) (Fig. 2). The proximal portion of the rachi on the wings are clearly defined; however, distally, feather preservation is poor (Fig. 2). There are two well-preserved contour feathers lying below the left wing where the rachi and barbs can be identified (Fig. 1c and 2a). Cu is distributed throughout the feathers with the most intensity proximally (Fig. 2a). As expected for bones (a hydroxyapatite), P is highly constrained to the bones and elevated relative to the entombing matrix (Fig. 2c). Ba, Ni, Mn, Cl and to a lesser extent, Br, are also associated within the feathers of AMNH FARB 30806.

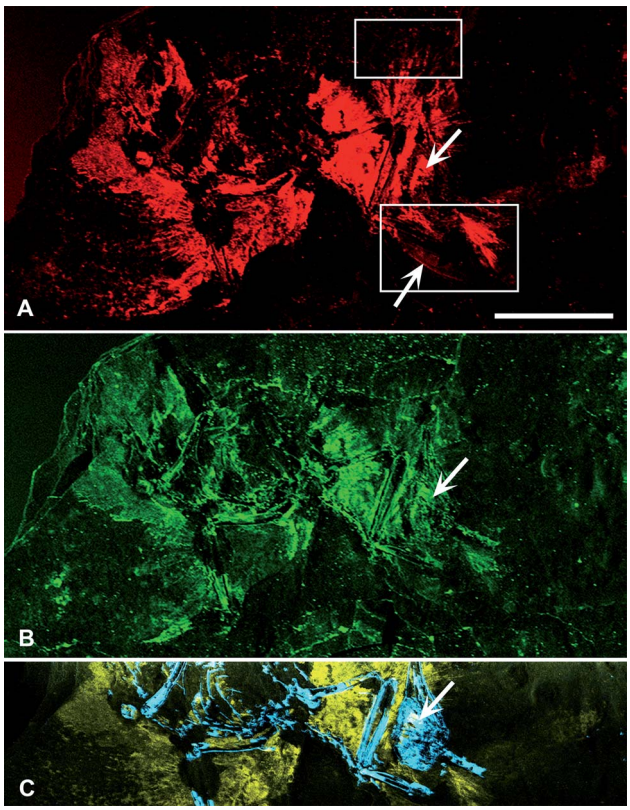

Fig. 2 SRS-XRF elemental maps of AMNH FARB 30806. (A) Copper (red) and (B) zinc (green) maps showing the relative intensities of the elements mapping distinctly within the feathers. (A) The upper box in copper corresponds to Fig. 1b, while the lower box corresponds to Fig. 1c. The lower arrow is pointing to the rachis of a feather. (C) Phosphorus (blue) and sulfur (yellow) elemental map distinctly showing bone with higher intensities of phosphorus and the feathers containing higher intensities of sulfur. (A–C) Upper arrow is pointing to the orbit (eye socket). Scale bar = 5 cm.

Quantification corroborates the maps and shows that P, S, Cl, Mn, Fe, Ni, Cu, Zn and Br are elevated in the feather regions compared to the matrix (Table 1). Additionally, there are elevated Mn, Ni, Cu, Zn, and Br within the orbit compared to the matrix. Lastly, P, S, Mn, Ni and Zn in bone show higher levels than in the matrix.

3.2. X-ray Absorption Near Edge Structure (XANES)

Sulfur XANES (Fig. 3) demonstrate the presence of 4 oxidation states for S: sulfate, sulfonate, sulfoxide and thiol. The more reduced forms of S (sulfonate, sulfoxide and thiol) appear only in preserved feathers and are not present in the matrix. Note that the peak above the sulfate energy for one of the matrix spectra (Fig. 3b) is most likely due a resonance feature at the Pb M_5 edge (Pb concentrations range between 65 and 83 ppm; see Table 1). This is likely a result of small amounts of Pb substituting for Ca in gypsum or anhydrite in the sedimentary matrix. When the S XANES spectra are normalized to raw intensity (I/I_0) based on the sulfate standard (Fig. 3f), the relative intensities of the different sulfur species in the matrix are appreciably lower than in any of the fossil feathers (Fig. 3). The relatively low organic peak in the matrix (Fig. 3b) could be the result of either hitting a small fragmentary fossil just below the surface of the matrix or of the breakdown and mass-transfer of organic S laterally from the fossil tissues. However, only sulfoxide is present so this might suggest a different source for this signal.

Copper XANES (Fig. 4) suggest that Cu is present as an organometallic chelate bound to organic O and/or N terminated functional groups in a similar manner to that seen in Wogelius *et al.*[8] and Manning *et al.*,[10] rather than as an inorganic compound such as Cu oxide. The Cu XANES spectra for AMNH FARB 30806 are similar to the eumelanin standard and previously published spectra from other Green River feathers (Fig. 4).[8] Both the Cu oxide and Cu foil produce additional peaks that are characteristic of inorganically bound Cu and are not seen in the Cu spectra for AMNH FARB 30806.

In contrast, Mn K-edge EXAFS taken from a feathered region (Fig. 1b) indicates that Mn is contained within an oxide precipitate. The local coordination environment of Mn is comparable to that for Mn contained in birnessite, a common mineral where Mn(IV) is in six-fold coordination with oxygen atoms at a distance of 1.874 angstroms. The strong second shell backscatter exhibited in the Fourier transform of EXAFS shown on Fig. 5 is completely different from the weak low amplitude feature that would be expected for a transition metal incorporated into an organometallic chelate. In this case the second shell is best fit by 6 Mn atoms at 2.869 atoms distance, consistent with birnessite or a slightly disordered birnessite group mineral. Taking account of a known birnessite three-legged multiple scattering path including O and Mn of ~3.3 angstroms length significantly improved the fit. The Mn mapped on the fossil feather is inorganic, and most likely results from post-mortem geochemical precipitation (Fig. 5).

Table 1 XRF point analyses. The numbers beside the feature correspond to the points marked on Fig. 1a. Beamline geometry is calibrated using a Durango apatite standard. 2σ errors, calculated from counting statistics, are approximately 8% relative for the light elements (Ca, Si, P, S, Cl) and 5% for all of the trace metals except Pb (for example, the Ca wt% in the bone is 37.9 ± 3% while the Zn concentration is 51 ± 2.6 ppm). Errors on Pb, due to overlap with As and rising background caused by the elastic and Compton scattering peaks, are much larger at approximately 25% (using the bone example: 64 ± 16 ppm)

High Z elements									Low Z elements				
	Element weight%		ppm W						Element weight%				
	Ca	Fe	Mn	Ni	Cu	Zn	As	Pb	Si	P	S	Cl	
Matrix	23.1	0.23	40	11	6	44	22	63	2.75	0.09	0.08	0.03	Matrix
Bone (2)	37.9	0.11	211	13	6	51	18	53	1.28	9.25	0.44	0.01	Bone (9)
Feather (1)	19.5	0.37	918	59	47	63	28	64	2.56	0.15	1.4	0.1	Feather (10)
Feather (3)	21.1	0.25	130	12	36	64	26	85	2.52	0.13	1.05	0.07	Feather (11)
Feather (5)	24.6	0.38	963	62	140	95	22	65	3.11	0.09	0.71	0.1	Feather (12)
Feather (6)	18.7	0.52	522	107	394	87	29	83					
Orbit	14.6	0.08	193	88	225	93	21	58					

3.3. Environmental Scanning Electron Microscopy (ESEM) with Energy Dispersive Spectroscopy (ESEM-EDS)

Both microscopy of the feathers and ESEM-EDS reveal a predominantly carbonaceous film with diagenetic crystalline mineral precipitates found throughout the feathers (Fig. 6). Elongate ovoids approximately 2 μm were also observed in a few discrete areas on the feathers (Fig. 6b and c). These structures are found on both the surface and within voids of the sedimentary rock. The ESEM-EDS spectra reveal more abundant C, S, Mg and Ti in the feather than within the matrix. In contrast, the matrix spectrum shows more abundant Ca, as expected in limestone in a carbonate rich rock.

4. Discussion

Synchrotron analyses show that there is a combination of endogenous and exogenous chemistry comprising AMNH FARB 30806. S, P, Cu and Zn can be mapped within discrete biological structures, *i.e.*, feathers and bone, indicating that these elements are most likely derived from the original biology of the organism (Fig. 2). Sulfur XANES shows that the S within the feathers is abundant and predominantly present as organically-bound, reduced forms that are either absent from or present in only minute quantities within the matrix (Fig. 3).

Copper is present as an organometallic chelate similar to that found in other studies where it has been interpreted as derived from eumelanin pigmentation and not as an inorganic species. Previous studies have found organic Cu occurring in different locations within a single feather[10] or within an entire bird.[8] Eumelanin dark pigmentation in animals and has been shown to chelate divalent trace metals such as Cu.[8,19,20] Concentrations of Cu in AMNH30806 feathers range from 36–394 ppm, while the matrix only contains 6 ppm (Table 1). The abundance and variability of Cu within the feathers suggests that the distribution of organic Cu relates to dark pigmentation of the feathers during life. However, due to the variable preservation of the feathers, especially in the wings, it is difficult to differentiate any patterning resulting from the relative intensities of Cu (Fig. 2a).

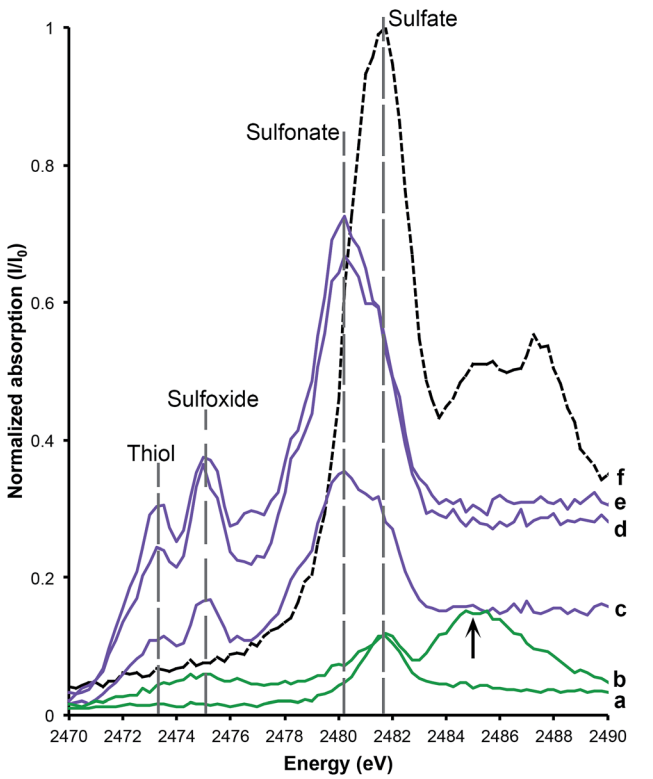

Fig. 3 Sulfur XANES for AMNH FARB 30806. The relative abundance of sulfur within the matrix (a and b) and feathers (c–e) has been calibrated to a sulfur standard, K_2SO_4 (f). The data are normalized to raw intensity I/I_0. The two matrix samples both have peaks that correspond with the sulfate standard, while the feathers contain abundant sulfonate, sulfoxide and thiol relative to the matrix samples. The lower matrix spectrum (a) shows an elongate organic peak across both sulfoxide and thiol due to the breakdown of organics. The upper matrix spectrum (b) has an additional peak at 2485 eV, which is due to Pb substitution for Ca in $CaSO_4$.

In combination with the SRS-XRF imaging, both the Cu and S XAS strongly indicate that these elements are derived from the original organism and have not been introduced from the surrounding environment during burial and subsequent fossilization. Correlation of Cu to total S shows an R^2 value of 0.57, a reasonably strong correlation after ~50 million years of burial. This high value is most likely due to S occurring in both the matrix and feathers as inorganic and organic species, respectively, whilst the Cu is contained only within the organic-rich areas of the feathers (Fig. 2 and 3). The correlation of organic S species to Cu is likely to be higher, as seen in previous studies,[5] as a function of chelated trace-metal from pigments inhibiting the breakdown of organic S rich keratin in the feather.[10] However, due to the large size of this specimen we were unable to map the entire fossil again below the sulfate critical energy to test this.

Phosphorus is constrained to the bones (Fig. 2c), as would be expected for hydroxyapatite, but is present in slightly lower quantities (~10 wt%) than expected for extant birds (~11–20 wt%).[21] Comparatively, P concentration within the matrix is less than 0.1 wt% (Table 1). Previous studies have shown that P loss from bones occurs within different geochemical environments[7,21] and this is likely the case in AMNH FARB 30806.

The feather preservation in AMNH FARB 30806 is variable, with some feathers well preserved, while others have clearly undergone more decomposition (Fig. 1). Fig. 1c shows one of the well-preserved feathers with gradational preservation from clear barbs to more patchy organic areas in the general form of feathers. This demonstrates differences in lateral preservation at the microfacies scale. This difference, although altering the morphological appearance of the feathers, does not appear to have a large impact on the preservation of mapped trace metals in the feathers (Fig. 2), supporting their relative immobility in preserved tissues (intact or degraded).

In addition to feathers, Cu and Zn are also concentrated within the orbit (eye) (Fig. 2a and b). The concentrations of these elements are elevated compared to the matrix but are within range of the feathers (Table 1). The elevated levels may either be due to underlying feathers or the original eye pigmentation. Avian eyes concentrate pigments in the vascular tunic (which includes the iris, choroid and ciliary body) the pecten oculi and the retinal pigment epithelium.[22] Many avian and non-avian dinosaur fossils from the Jehol Biota of North

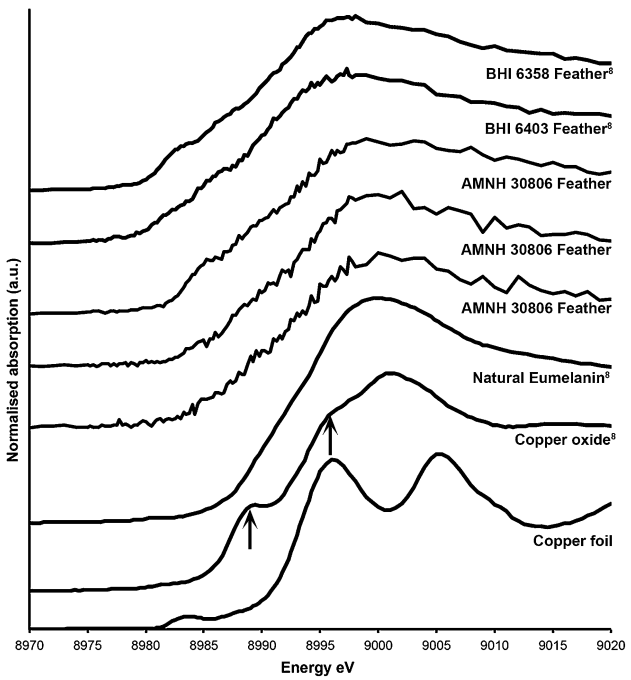

Fig. 4 Copper XANES spectra. Cu XANES spectra are from a copper standard (copper foil) and three different feathers from AMNH FARB 30806. The spectra from these have been plotted along with published spectra from copper oxide, natural copper eumelanin, and two isolated feathers from the Green River Formation (BHI 6358 and 6403).[8] The arrows on the copper oxide are pointing to peaks that are unique to that spectrum and do not occur in the fossil material.

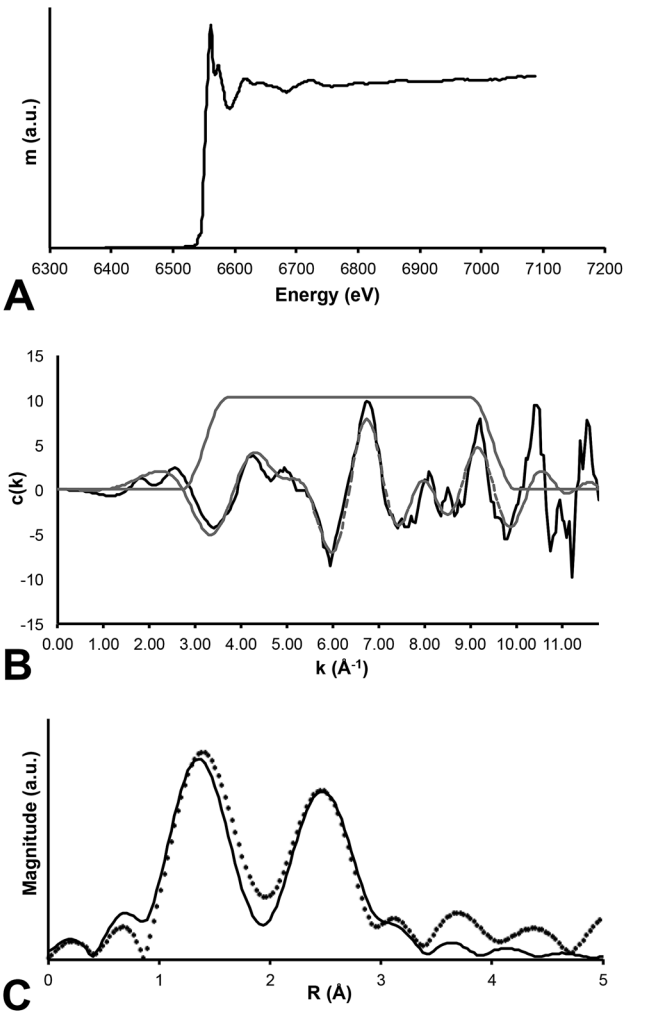

Fig. 5 Mn EXAFS. Three panel results of EXAFS analysis of Mn within the fossil specimen. (A) Raw data for the absorption coefficient measurement at the Mn K-edge. (B) EXAFS function presented for the specimen (solid line) and a computed fit to the data (dashed line). (C) Fourier transform of EXAFS where the data are presented as the discrete points and the best fit is shown as the thin solid line. Clearly the RDF shows two strong backscattering shell surrounding the central Mn absorber.

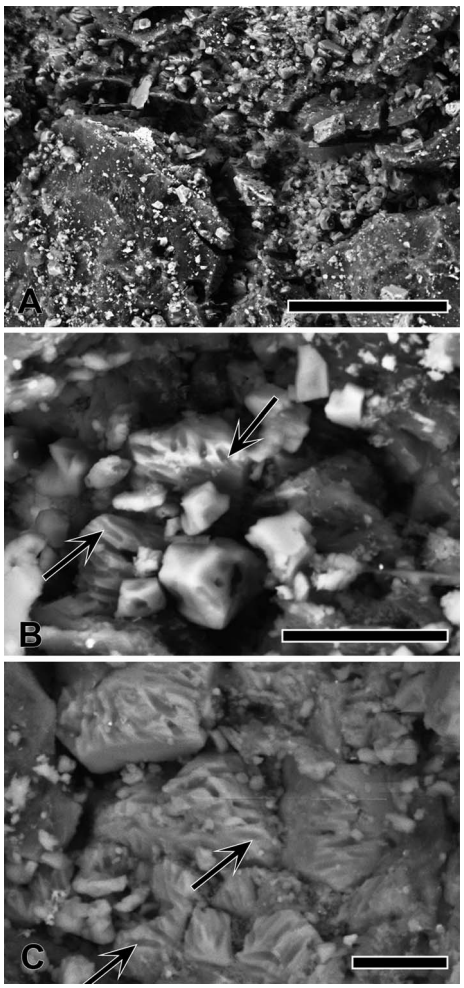

Fig. 6 SEM of feathers from AMNH FARB 30806. (A) Secondary electron image of a carbonaceous film, mineral crystals and possible eumelanosomes (arrow). Scale bar = 50 μm. (B) Backscattered electron image of possible eumelanosome preservation (arrow). Scale bar = 10 μm. (C) Secondary electron image of possible eumelanosome preservation (arrow). Scale bar = 5 μm.

Eastern China display large amounts of preserved pigment inside the orbits.[23] It has been suggested that one of the functions of melanosomes within pigmented portions of the eye include acting as a barrier against sustained exposure to both visible and ultraviolet light as well as protection against oxygen radicals.[22,24,25] Elevated levels of Zn, in particular, have been shown to be an important antioxidant and to help moderate light levels among other physiological functions.[26] Melanosomes have been previously reported in the eyes of a fossil bird,[27] mosasaur[28] and fish.[8,29]

Manganese is among several metallic elements that are known porphyrin chelates in melanin[19,20] but is also extremely common in geochemical systems. Initially, the distribution of Mn in AMNH FARB 30806 appears to follow biological structures in a similar manner to Cu and S (Fig. 7). This could be interpreted as Mn being derived from melanin. However, the Mn EXAFS presented here show Mn is present as an inorganic oxide (Fig. 5). Thus, the presence of Mn in fossils may not necessarily indicate geochemical precipitation post-burial. Reduced fluids most likely flowed through the slightly more permeable bed containing the fossil and became oxidized in the void space due to the presence of slightly elevated oxygen levels. This would oxidize soluble Mn(II) to insoluble Mn(IV) and cause the Mn-oxides to nucleate on the fossil material. This result shows the importance of XAS analysis in partnering with the imaging data so as to differentiate inorganic precipitates from biologically derived material.

ImageJ correlation analyses between selected elements also strongly indicates precipitation of inorganic compounds post burial. Ba is indicative of inorganic precipitates and its correlation with Mn ($R^2 = 0.80$) and Ni ($R^2 = 0.68$) supports that these other two elements may also be inorganically derived and may be part of the same phase of elemental influx. In previous studies Ni has been proposed to be endogenous in fossil birds based on correlation with Cu and organic S[10]. However, this does not suggest that elevated Ni concentration in all cases is exclusively either organically or inorganically derived. Rather, different taphonomic processes may result in variable preservation, alteration, removal and precipitation of certain trace metals. The relative location of Ba, Ni and Mn along the bones and feather rachides suggests that these biological structures allowed for a preferential diagenetic fluid path. This, in turn, allowed for the precipitation of these elements in addition to others such as Br and Cl. A number of cases of geochemical precipitation within fossil specimens have been discussed previously (*e.g.* Bergmann *et al.*[7]), this particular specimen however provided a unique test of our methodology because the Mn precipitates so closely mimicked the biological structures.

Many previous studies on fossil pigments have focused on the melanin pigment containing organelles, melanosomes (*e.g.* Vinther *et al.*,[27] Clarke *et al.*,[30] Li *et al.*,[31] Zhang *et al.*,[32] Barden *et al.*,[33] Carney *et al.*,[34] Glass *et al.*,[35] McNamara[36]). The majority of the feathers examined show a desiccated carbonaceous film with diagenetic mineral crystals (Fig. 6). In AMNH FARB 30806 there is little evidence of possible eumelanosomes (elongate organelles associated with dark pigmentation) and no phaeomelanosomes (circular organelles associated with light pigmentation) (Fig. 6b and c). The putative eumelanosomes

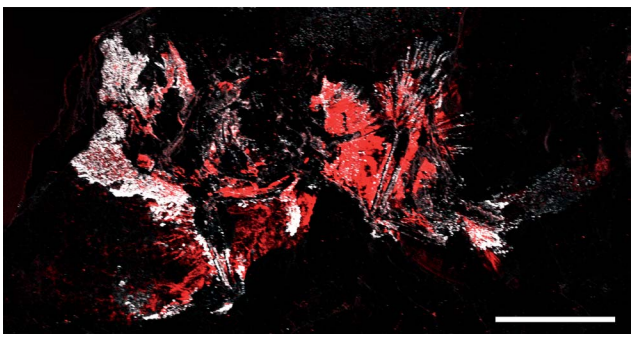

Fig. 7 Copper and manganese elemental map of AMNH FARB 30806. Copper (red) and manganese (white) both appear to map within the feathers; however correlation between the two show no significance in the distribution. Scale bar = 5 cm.

appear as external moulds of the elliptical organelles; however, due to the advanced degradation of the feathers in AMNH FARB 30806, it is difficult to ascertain whether these structures occur within the feather or within the sediment. Identifying the location of these structures is important, as one of the only ways to differentiate between melanosomes and morphologically similar bacteria, is the location (*i.e.*, inside the keratinous sheath or outside, respectively) of the structures.[37] ESEM-EDS results show S being present within the moulds; however EDS cannot determine S oxidation state and so this S could either have an organic or inorganic affinity. The Cu SRS-XRF maps show that there is Cu present in the feathers analyzed under ESEM (Fig. 2a, upper box) but the resolution was not enough to identify any organelles. Therefore, it is inconclusive whether the ellipsoidal structures are external moulds of eumelanosomes or some other organic product. The presence of C and S that maps within discrete biological structures might either be a function of endogenous tissue preservation or possible bacterially mediated exogenous overprint, albeit both due to biological processes.

5. Conclusion

The preservation of soft tissues in fossils is a function of the interplay between biochemical and geochemical processes within a complicated series of events that begin at the moment of death. AMNH FARB 30806, although well preserved, may not necessarily be considered to be exceptional, but nonetheless provides important information on the taphonomy of birds in the Green River Formation. Upon visual inspection, the feathers appear to be poorly preserved with some rachi and barbs definable and only two distinct individual feathers. However, elemental maps show that some endogenous elements reduce the ambiguity of biological structures, such as P in the bone and S and Cu in the feathers. The local coordination chemistry of S and Cu show that they are organically bound, most likely from the remnants of keratin and eumelanin, respectively. Unlike other specimens[10] where geochemically sourced elements do not correlate with biological structures, the geochemical association in AMNH FARB 30806 is much stronger. This study has been able to clearly differentiate between organic remains from those overprinted by geochemical precipitates. In particular, Mn has been revealed as an Mn oxide, birnessite or closely related mineral, rather than an organometallic chelate even though it appears to be distributed within biological structures. Additional exogenous elements include Ba, Br and Ni that map along the bones and feathers, with the organic remains acting as nucleation sites for the geochemical precipitates. Finally, careful analysis must be conducted in order to accurately unpick the taphonomic history of fossils, using the quantification and distribution of chemistry to provide insight to the biology and biochemistry of ancient life.

Acknowledgements

We would like to thank Carl Mehling from the American Museum of Natural History for his help in the preservation of this fossil. We would also like to thank Dr Karen Rosenthal for her helpful discussions on avian anatomy and physiology. Additionally, we would like to thank NERC (grant number NE/J023426/1), STFC, Diamond Lightsource and SLAC National Accelerator Laboratory for their support. Portions of this work have been carried out at the Stanford. Synchrotron Radiation Lightsource, a National User Facility operated by Stanford University on behalf of the U.S. Department of Energy, Office of Basic Energy Sciences.

References

1 A. K. Behrensmeyer, S. M. Kidwell, R. A. Gastaldo, D. H. Erwin and S. L. Wing, *Paleobiology*, 2000, **26**, 103–147.
2 A. K. Behrensmeyer, in *Taphonomy: Releasing the Data Locked in the Fossil Record*, ed. P. A. Allison and E. G. Briggs, Plenum Press, New York, 1991, vol. 9, ch. 6, pp. 291–335.
3 P. L. Manning, P. M. Morris, A. McMahon, E. Jones, A. Gize, J. H. S. Macquaker, G. Wolff, A. Thompson, J. Marshall, K. G. Taylor, T. Lyson, S. Gaskell, O. Reamtong, W. I. Sellers, B. E. van Dongen, M. Buckley and R. A. Wogelius, *Proc. R. Soc. B*, 2009, DOI: 10.1098/rspb.2009.0812.
4 L. Grande, *The Lost World of Fossil Lake: Snapshots from the Past*, The University of Chicago Press, 2013.
5 N. P. Edwards, P. Manning, U. Bergmann, P. Larson, B. E. van Dongen, W. I. Sellers, S. M. Webb, D. Sokaras, R. Alonso-Mori, K. Ignatyev, H. E. Barden, A. van Veelen, J. Anné, V. M. Egerton and R. A. Wogelius, *Metallomics*, 2014, **6**, 774–782.
6 N. P. Edwards, R. A. Wogelius, U. Bergmann, P. Larson, W. I. Sellers and P. L. Manning, *Appl. Phys. A: Mater. Sci. Process.*, 2013, **111**, 147–155.
7 U. Bergmann, R. W. Morton, P. L. Manning, W. I. Sellers, S. Farrar, K. G. Huntley, R. A. Wogelius and P. Larson, *Proc. Natl. Acad. Sci. U. S. A.*, 2010, **107**, 9060–9065.
8 R. A. Wogelius, P. L. Manning, H. E. Barden, N. P. Edwards, S. M. Webb, W. I. Sellers, K. G. Taylor, P. L. Larson, P. Dodson, H. You, L. Da-qing and U. Bergmann, *Science*, 2011, **333**, 1622–1626.
9 N. P. Edwards, H. E. Barden, B. E. van Dongen, P. L. Manning, P. L. Larson, U. Bergmann, W. I. Sellers and R. A. Wogelius, *Proc. R. Soc. B*, 2011, **278**, 3209–3218.
10 P. Manning, N. P. Edwards, R. A. Wogelius, U. Bergmann, H. E. Barden, P. Larson, D. Schwarz-Wings, V. M. Egerton, D. Sokaras, R. A. Mori and W. I. Sellers, *J. Anal. At. Spectrom.*, 2013, **28**, 1024–1030.
11 J. Anné, N. P. Edwards, R. A. Wogelius, A. R. Tumarkin-Deratzian, W. I. Sellers, A. van Veelen, U. Bergmann, D. Sokaras, R. Alonso-Mori, K. Ignatyev, V. M. Egerton and P. L. Manning, *J. R. Soc., Interface*, 2014, **11**.
12 U. Bergmann, P. L. Manning and R. A. Wogelius, *Annu. Rev. Anal. Chem.*, 2012, **5**, 361–389.
13 C. A. Schneider, W. S. Rasband and K. W. Eliceiri, *Nat. Methods*, 2012, **9**, 671–675.
14 G. Chinga and K. Syverud, *Nord. Pulp Pap. Res. J.*, 2007, **22**, 441–446.

15 J. J. Rehr and R. C. Albers, *Rev. Mod. Phys.*, 2000, **72**, 621–654.
16 V. A. Solé, E. Papillon, M. Cotte, P. Walter and J. Susini, *Spectrochim. Acta, Part B*, 2007, **62**, 63–68.
17 M. Sandström, F. Jalilehvand, E. Damian, Y. Fors, U. Gelius, M. Jones and M. Salomé, *Proc. Natl. Acad. Sci. U. S. A.*, 2005, **102**, 14165–14170.
18 K. M. Wetherall, R. M. Moss, A. M. Jones, A. D. Smith, T. Skinner, D. M. Pickup, S. W. Goatham, A. V. Chadwick and R. J. Newport, *J. Archaeol. Sci.*, 2008, **35**, 1317–1328.
19 G. E. Hill and K. J. McGraw, *Bird Coloration: Mechanisms and measurements*, Harvard University Press, 2006.
20 M. Niecke, M. Heid and A. Krüger, *J. Ornithol.*, 1999, **140**, 355–362.
21 M. B. Goodwin, P. G. Grant, G. Bench and P. A. Holroyd, *Palaeogeogr., Palaeoclimatol., Palaeoecol.*, 2007, **253**, 458–476.
22 M. P. Jones, K. E. Pierce Jr and D. Ward, *J. Exot. Pet Med.*, 2007, **16**, 69–87.
23 *The Jehol Fossils: The Emergence of Feathered Dinosaurs, Beaked Birds and Flowering Plants*, ed. P.-j. Chen, Y. Wang, Y.-q. Wang and M.-M. Chang, Academic Press, London, 2008.
24 S. G. Kiama, J. Bhattacharjee and K. D. Weyrauch, *J. Anat.*, 1994, **185**, 637–642.
25 D.-N. Hu, J. D. Simon and T. Sarna, *Photochem. Photobiol.*, 2008, **84**, 639–644.
26 B. H. Grahn, P. G. Paterson, K. T. Gottschall-Pass and Z. Zhang, *J. Am. Coll. Nutr.*, 2001, **20**, 106–118.
27 J. Vinther, D. E. G. Briggs, R. O. Prum and V. Saranathan, *Biol. Lett.*, 2008, **4**, 522–525.
28 J. Lindgren, M. W. Caldwell, T. Konishi and L. M. Chiappe, *PLoS One*, 2010, **5**, e11998.
29 J. Lindgren, P. Uvdal, P. Sjövall, D. E. Nilsson, A. Engdahl, B. P. Schultz and V. Thiel, *Nat. Commun.*, 2012, **3**, 824.
30 J. A. Clarke, D. T. Ksepka, R. Salas-Gismondi, A. J. Altamirano, M. D. Shawkey, L. D'Alba, J. Vinther, T. J. DeVries and P. Baby, *Science*, 2010, **330**, 954–957.
31 Q. Li, K.-Q. Gao, J. Vinther, M. D. Shawkey, J. A. Clarke, L. D'Alba, Q. Meng, D. E. G. Briggs and R. O. Prum, *Science*, 2010, **327**, 1369–1372.
32 F. Zhang, S. L. Kearns, P. J. Orr, M. J. Benton, Z. Zhou, D. Johnson, X. Xu and X. Wang, *Nature*, 2010, **463**, 1075–1078.
33 H. E. Barden, R. A. Wogelius, D. Li, P. L. Manning, N. P. Edwards and B. E. van Dongen, *PLoS One*, 2011, **6**, e25494.
34 R. M. Carney, J. Vinther, M. D. Shawkey, L. D'Alba and J. Ackermann, *Nat. Commun.*, 2012, **3**, 637.
35 K. Glass, S. Ito, P. R. Wilby, T. Sota, A. Nakamura, C. Russell Bowers, K. E. Miller, S. Dutta, R. E. Summons, D. E. G. Briggs, K. Wakamatsu and J. D. Simon, *Org. Geochem.*, 2013, **64**, 29–37.
36 M. E. McNamara, *Palaeontology*, 2013, **56**, 557–575.
37 A. E. Moyer, W. Zheng, E. A. Johnson, M. C. Lamanna, D.-q. Li, K. J. Lacovara and M. H. Schweitzer, *Sci. Rep.*, 2014, **4**.